Journal of Superconductivity and Novel Magnetism
https://doi.org/10.1007/s10948-024-06759-w

RESEARCH

Structural, Magnetic, Morphology, Optical, and Vibrational Properties of In Substituted La_2CuO_4 Nanoparticles

M. Sundararajan[1] · P. Aji Udhaya[2] · S. Baskar[3] · Mohd Ubaidullah[4] · Manish Gupta[5] · S. Yuvaraj[6] · Chandra Sekhar Dash[7] · Kirtanjot Kaur[8] · Ala Manohar[9] · R. S. Rimal Isaac[10] · Shoyebmohamad F. Shaikh[4]

Received: 18 January 2024 / Accepted: 6 May 2024

Abstract

Perovskite type nanocrystals of $La_{2-x}In_xCuO_4$ were prepared by using the combustion method. The magnetic, optical, morphology, structural, and vibrational characteristics were investigated using techniques like XRD, FE-SEM, FTIR, VSM, EDX, and DRS-UV. The development of the pure La_2CuO_4 perovskite structure was established by XRD analysis. When there is an increase in the indium ion concentration ($x = 0.00$ to 0.25), orthorhombic phase takes place. The orthorhombic structure crystallite size is from 54 to 38 nm, respectively. The oxidation states of the synthesized nanoparticles were carried out via X-ray photoelectron spectroscopy (XPS). TG-DTA studies confirmed weight loss and exothermic transitions. Because of quantum confinement phenomena, the direct band gap energy increases with an increase in In^{3+} ion content (1.70 to 1.73 eV) and that was calculated using the Kubelka–Munk method. The La_2CuO_4 system demonstrates the formation of nanoscale crystalline grains with fused grain boundaries, resulting in the presence of pores and pore walls. The magnetization-field method yields hysteresis curves at room temperature (RT) that indicate the existence of ferro/paramagnetic characteristics.

Keywords Nanocrystals of $La_{2-x}In_xCuO_4$ · Magnetic and optical properties · Structural and elemental properties · Combustion technique

1 Introduction

Perovskite substances provide numerous benefits as a consequence of their distinct properties and enormous application in the areas of photo-electrochemical disintegration of water, catalyst, gas sensor, superconductor [1–4], and so on. Lanthanum–copper oxide is an example for mixed metal oxide whose structure is similar to perovskites. The said structure expresses the recurring layering of cation A (larger, 9-fold coordination) parted with rock-salt (AO) and perovskite

✉ Mohd Ubaidullah
mtayyab@ksu.edu.sa

✉ S. Yuvaraj
phyuvaraj@gmail.com

✉ Chandra Sekhar Dash
chandu0071@gmail.com

1 PG & Research Department of Physics, Paavendhar College of Arts & Science, M.V. South, Thalaivasal, Salem, Tamil Nadu 636 121, India

2 Department of Physics, Holy Cross College (Autonomous), Nagercoil, Affiliated to Manonmanium Sundaranar University, Tirunelveli, Tamil Nadu, India

3 Department of Physics, KG Reddy College of Engineering and Technology, Moinabad, Hyderabad, India

4 Department of Chemistry, College of Science, King Saud University, P.O. Box 2455, Riyadh 11451, Saudi Arabia

5 Division of Research and Development, Lovely Professional University, Phagwara, Punjab, India

6 Department of Physics, Vel Tech Rangarajan Dr. Sagunthala R&D Institute of Science and Technology, Vel Nagar, Avadi, Chennai 600 062, Tamil Nadu, India

7 Department of Electronics and Communication Engineering, Centurion University of Technology and Management, Bhubaneswar 752050, Odisha, India

8 University Centre for Research and Development, Chandigarh University, Mohali 140413, India

9 Department of Physics, Yeungnam University, Gyeongsan 38541, Republic of Korea

10 Department of Nanotechnology, Noorul Islam Centre for Higher Education, 629180 Kumaracoil, Kanyakumari District, Tamil Nadu, India

Published online: 24 May 2024

(ABO_3) and cation B which is smaller (octahedral coordination) [5]. La_2CuO_4 (LC) system is a type of cuprate structure with a K_2NiF_4 model mono-layered structure. That system is represented as a pile up of single-plane cupric oxide layers, which are separated by lanthanum oxide layers [6]. The conversion of the LC system from a p-type semiconductor with antiferromagnetic properties to a superconductor may be achieved by displacing lanthanum ions with rare earth cations such as barium, strontium, and calcium, or by injecting more O_2 into the interstitial sites.

In several oxidation and reduction reactions [1], the LC system, which is a type of robust material, is used. By applying pressure, changing the temperature, or doping concentration, the structure phase transition of the semi-conducting LC system takes place from orthorhombic to tetragonal [7–9]. The LC metal oxide shows three significant structural phases, namely (i) HTT (high temperature tetragonal), (ii) LTT (low temperature tetragonal), and (iii) LTO (low temperature orthorhombic) with $P4_2/ncm$, I_4/mmm, and *Bmab* symmetry [10, 11]. Various physical and chemical methods like solid state [6], combustion [2], co-precipitation method [3], hydrothermal [12], and sol-gel [1] can be used to prepare the LC nanoparticles. The objective of this study is to synthesize La_2CuO_4 and introduce In^{3+} doping into La_2CuO_4 systems using the combustion method. The synthesized samples are subsequently characterized using various techniques, viz. XPS, TG/DTA, FE-SEM, VSM, XRD, EDX, FTIR, and DRS. These techniques will be used to evaluate the elemental composition, optical band gap, vibrational frequencies, structural stretching frequencies, magnetic properties, and surface morphology of the system, respectively [12–14].

2 Experimental

2.1 Preparation of $La_{2-x}In_xCuO_4$ Nanoparticles

The regents used were of analytical quality, sourced from SD fine chemicals in India, and were employed without any further purification. Precursors such as lanthanum nitrate, copper nitrate, and indium nitrate were used, with L-alanine acting as the fuel. The La_2CuO_4 (LC) compound was synthesized in its pure form, as well as in compositions doped with In^{3+} ions. Indium was added at various mole ratios ($x = 0$, 0.05, 0.15, and 0.25) to the La_2CuO_4 system. The components were dissolved in de-ionized water in the necessary ratio (2:1) and stirred for 45 min at RT to get a uniform solution. The homogenous solution was placed in a hot air oven and maintained at a temperature of 110 °C for 60 min. At first, the solution was heated and dried, resulting in its breakdown and the release of gases. The combustion process was fueled by L-alanine, with the nitrates in the precursors serving as the oxidizers. The fuel to oxidation ratio (F/O) was precisely 1, by the principles of propellant chemistry. Upon reaching the stage of spontaneous combustion, the solution underwent ignition, leading to the fast formation of flames and the production of the ultimate products. After the reaction and annealing process, the samples were thoroughly rinsed with distilled water before being dried in a hot air oven at a temperature of 750 °C for 90 min. The powders obtained using various concentrations of In^{3+} ($x = 0$, 0.05, 0.15, and 0.25) were labeled as La_2CuO_4, $La_{1.95}In_{0.05}CuO_4$, $La_{1.85}In_{0.15}CuO_4$, and $La_{1.75}In_{0.25}CuO_4$, labeled as a, b, c, and d, respectively.

2.2 Sample Characterizations

The LC system utilized an X-ray diffractometer (RIGAKU ULTIMA VI) with an emission at = 1.5406 Å (with Cu-Kα) for 2θ values ranging from 20 to 80° to determine the substances' structure. Thermal analysis was performed by thermogravimetric/differential thermal analysis (PERKIN-ELMER). The surface analysis of La_2CuO_4 and In doped La_2CuO_4 nanoparticles were recorded via XPS (KRATOS-AXIS Ultra DLD) having AlKα radiation (1486.6 eV) ran at 10 mA /13 KeV with 160 eV energy and 20 eV resolution, and the system was calibrated through referencing of 1 s carbon peak (285.0 eV). The surface functional groups were determined through the utilization of a Thermo Scientific NICOLET iS10 OMNI FTIR spectrophotometer. Utilizing a THERMO SCIENTIFIC EVOLUTION 300 UV-visible spectrophotometer, which records diffuse reflectance UV-visible spectra, the optical band gap energy was ascertained. The elemental composition study was conducted by reporting the surface analysis of the substance at the desired magnification using an HITACHI S4800 HR-field scanning electron microscope (FE-SEM) outfitted with a HORIBA EMAX energy dispersive X-ray (EDX) source. The magnetic properties of the sample were ascertained utilizing a vibrating sample magnetometer (PMC MICROMAG 3900 MODEL) equipped with a 1T magnet operating at ambient temperature. At ambient temperature, magnetization loops have been measured between −15,000 Oe and 15,000 Oe.

3 Results and Discussion

3.1 X-ray Diffraction Analysis

Pure La_2CuO_4 and In doped La_2CuO_4 showed a single-phase perovskite like (A_2BO_4) orthorhombic structure with space group *Bmab* (JCPDS No: 88–0940) is shown in Fig. 1. The diffraction peaks at 2θ values around 24.26°, 27.07°, 30.98°, 33.01°, 33.48°, 41.04°, 41.65°, 43.37°, 47.75°, 53.87°, 54.31°, 55.72°, 58.06°, 64.78°, 65.09°, 69.65°, 69.93°, 75.25°, 76.50°,

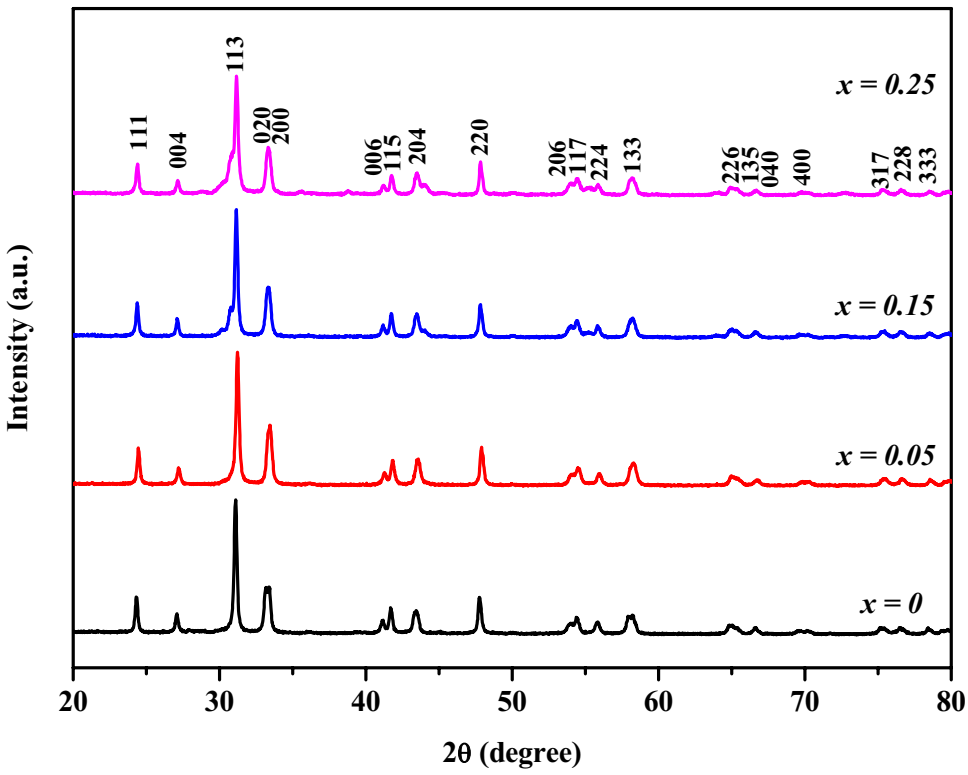

Fig. 1 Pure La_2CuO_4 and In doped La_2CuO_4 showed a single-phase perovskite like (A_2BO_4) orthorhombic structure with space group Bmab (JCPDS No: 88–0940)

and 78.37° are mapped to 111, 004, 113, 020, 200, 006, 115, 204, 220, 206, 117, 224, 133, 226, 135, 040, 400, 317, 228, and 333 crystallographic planes, respectively [13, 14].

By using the X-ray diffraction pattern method, the orthorhombic LC sample lattice parameters were determined, and the Eq. (1) is given below.

$$\frac{1}{d^2} = \frac{h^2}{a^2} + \frac{k^2}{b^2} + \frac{l^2}{c^2} \tag{1}$$

where inter-atomic spacing is given by the letter *d*, and the lattice constants are represented by the constants *a*, *b*, and *c*. Table 1 shows lattice parameters a, b, and c. It is discovered that the values for a, b, and c decrease with a rise in indium addition from $x = 0$ to 0.25, and that for *c*, the value decreases. Even though the radius of La^{3+} ion ($r_{La}{}^{3+} = 1.06$ Å) is higher than that of the In^{3+} ion ($r_{In}{}^{2+} = 0.81$ Å), there is a decrease in the lattice parameter values (*a*, *b*, and *c*) due to the ionic radius of indium.

Table 1 Sample code, crystallite size, lattice parameter, Rietveld refinement factors, and band gap values of $La_{2-x}In_xCuO_4$ ($x = 0.0$, 0.05, 0.15, and 0.25) samples

Sample	Sample code	Crystallite size, L (nm)	Lattice parameter, a, b, and c (Å)	Fit parameters	Energy gap (eV)
La_2CuO_4	a	54	5.834 5.841 13.146	$R_{wp} = 6.33$ $R_p = 4.92$ $R_e = 5.84$ S = 1.08	1.70
$La_{1.95}In_{0.05}CuO_4$	b	49	5.826 5.831 13.140	$R_{wp} = 6.41$ $R_p = 4.98$ $R_e = 5.92$ S = 1.07	1.71
$La_{1.85}In_{0.15}CuO_4$	c	43	5.820 5.823 13.133	$R_{wp} = 7.73$ $R_p = 5.68$ $R_e = 5.96$ S = 1.05	1.72
$La_{1.75}In_{0.25}CuO_4$	d	38	5.811 5.815 13.125	$R_{w\,p} = 7.44$ $R_p = 5.75$ $R_e = 5.63$ S = 1.03	1.73

From the Debye–Scherrer formula, the LC sample's average crystallite size has been computed employing this Eq. (2).

$$D = \frac{0.89\lambda}{\beta \cos\theta} \tag{2}$$

where λ is the X-ray wavelength, θ is the Bragg diffraction angle, β is the full width at half maximum (FWHM), and D is the crystallite size. It is determined that LC samples exhibit the average crystallite size (54 nm), while that of the substances doped with In^{3+} ranges from 54 to 38 nm shows a lower crystallite size, which is an increase in the concentration of indium ion from $x = 0.05$ to 0.25 as depicted in Table 1.

The Rietveld refinement investigations of the La_2CuO_4 system, as seen in Fig. 2, were conducted using the FULLPROF software. The refining was conducted in the Bmab space group. The X-ray diffraction (XRD) pattern of the samples exhibits a strong agreement with the predicted pattern. Figure 2 indicates a complete alignment between the observed and estimated profile patterns. The analysis validated the presence of the perovskite structure in the samples. The χ^2 values for all the LC system samples provided in Table 1 show a proximity to 1. The goodness of fit parameter (S) is $S = R_{wp}/R_e$, where R_{wp} and R_e are the weighted profile and predicted weighted profile reliability factors. "S" at roughly 1 indicates a good match and confirms that the refinement parameters were estimated more precisely [14].

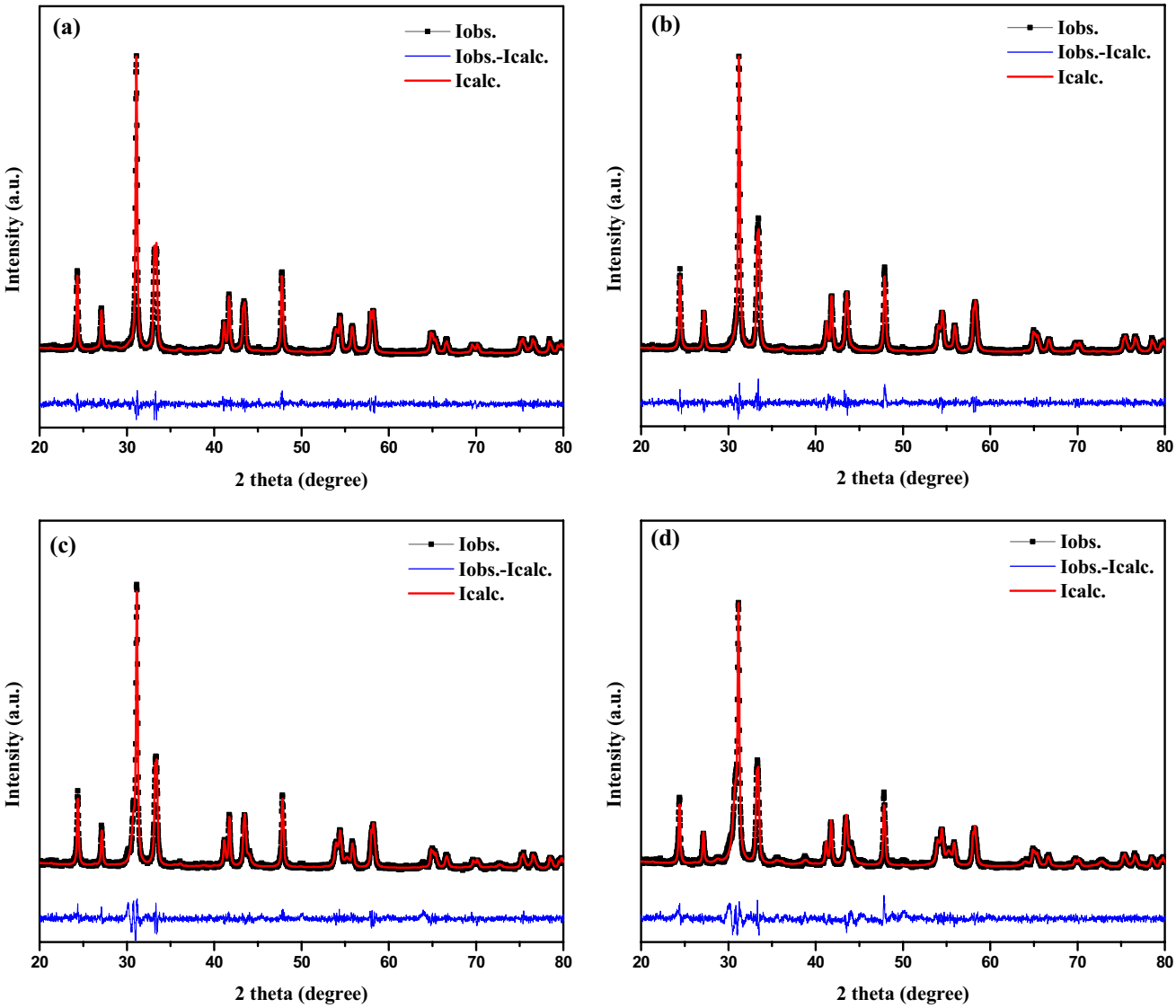

Fig. 2 The Rietveld refinement investigations of the La_2CuO_4 system

3.2 XPS Analysis

To study the structural and chemical bonding characteristics of the La_2CuO_4 and In doped La_2CuO_4 nanoparticles, XPS analysis was performed. Figure 3 shows the wide spectra of elements such as La 3d, In 3d, Cu 2p, O 1s, and C, respectively. In Fig. 3a, the peaks at 837.83 and 833.84 eV and 851.52 and 854.71 eV are La 3d peaks that are related to La $3d_{5/2}$ and La $3d_{3/2}$, respectively [15]. In Fig. 3b at 450. 96 and 442.36 eV are related to In $3d_{3/2}$ and In $3d_{5/2}$, and

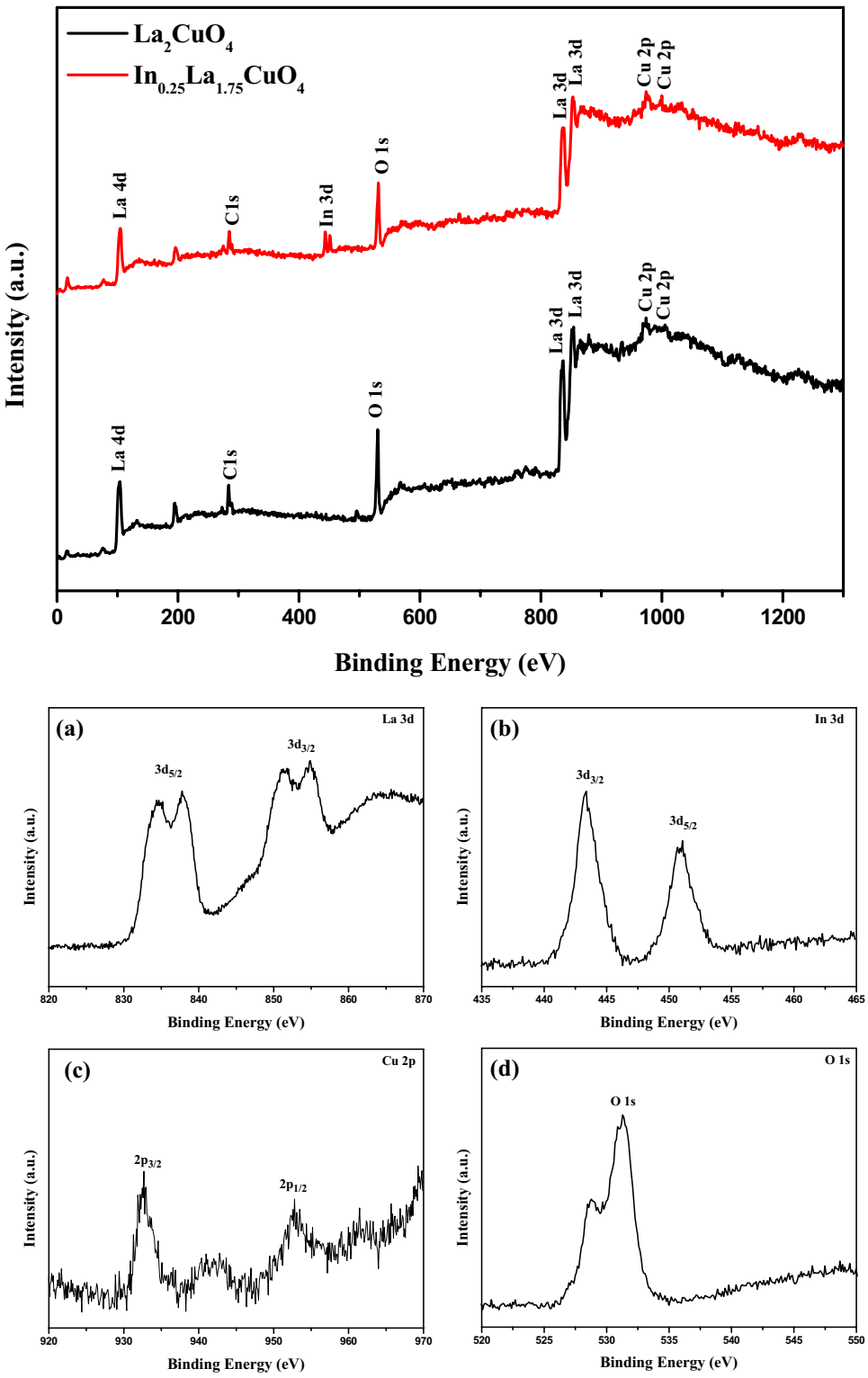

Fig. 3 The wide spectrum of elements La_2CuO_4 and In doped La_2CuO_4 **a** La 3d, **b** In 3d, **c** Cu2p, **d** O 1s

this confirms the presence of indium in the In^{3+} state [16]. Cu's $2p_{3/2}$ and $2p_{1/2}$ states correspond to binding energies of 952.78 eV and 932.78 eV, respectively, and are connected to $2p_{1/2}$ and In $2p_{3/2}$, which exhibit spin-orbital interaction (see Fig. 3c). Furthermore, Cu occurs in the Cu^{2+} state, as evidenced by satellite peaks at 961.89 eV and 942.50 eV [17]. In Fig. 3d, the peak at 528.73, 529.73, and 531.21 eV indicates the existence of O 1s after a limited XPS scan, providing the binding energy of O^{2-} in the crystal lattice. The binding energies were calculated using the C 1s line at 284.6 eV, which appeared in a wide range of spectra. The XPS spectra demonstrate that In-doped La_2CuO_4 nanoparticles were effectively prepared. We performed XPS to study the cation distribution, which was found to be aligned with their atomic % formula, having In^{3+}, La^{3+}, and Cu^{2+} cations.

3.3 TG-DTA Analysis

To study the thermal characteristics of the prepared pure and In doped La_2CuO4 nanoparticles, TG-DTA study is performed by varying the temperature in the range of RT to 800 °C. During the process, the N_2 gas is employed as ambient gas. TG curves of pure and In doped La_2CuO_4 nanoparticles are depicted in Fig. 4, which disclosed two distinct stages of weight loss. The first stage of weight loss was determined to be 0.6, 0.3, 0.1, and 0.06% ($0 \le x \le 0.25$) throughout the temperature range of 33–83 °C, which attributed to the removal of water molecules, corresponding to an endothermic transition as depicted in the DTA curve [18]. The breakdown of the organic component is responsible for the second stage of weight loss, which was determined to be 3.4%, 2.9, 2.2, and 1.1% ($0 \le x \le 0.25$), between the temperature range of 307–364 °C. This stage of weight loss is very well matched with the exothermic transition noticed in the DTA curve. Therefore, it was discovered that the total weight loss for ferrite nanoparticles that were produced was 4, 3.2, 2.3, and 1.16%. A weight loss of no more than 569 °C, 541 °C, 538 °C, and 511 °C is discovered, indicating that pure and In doped La_2CuO_4 nanoparticles are thermally stable [19].

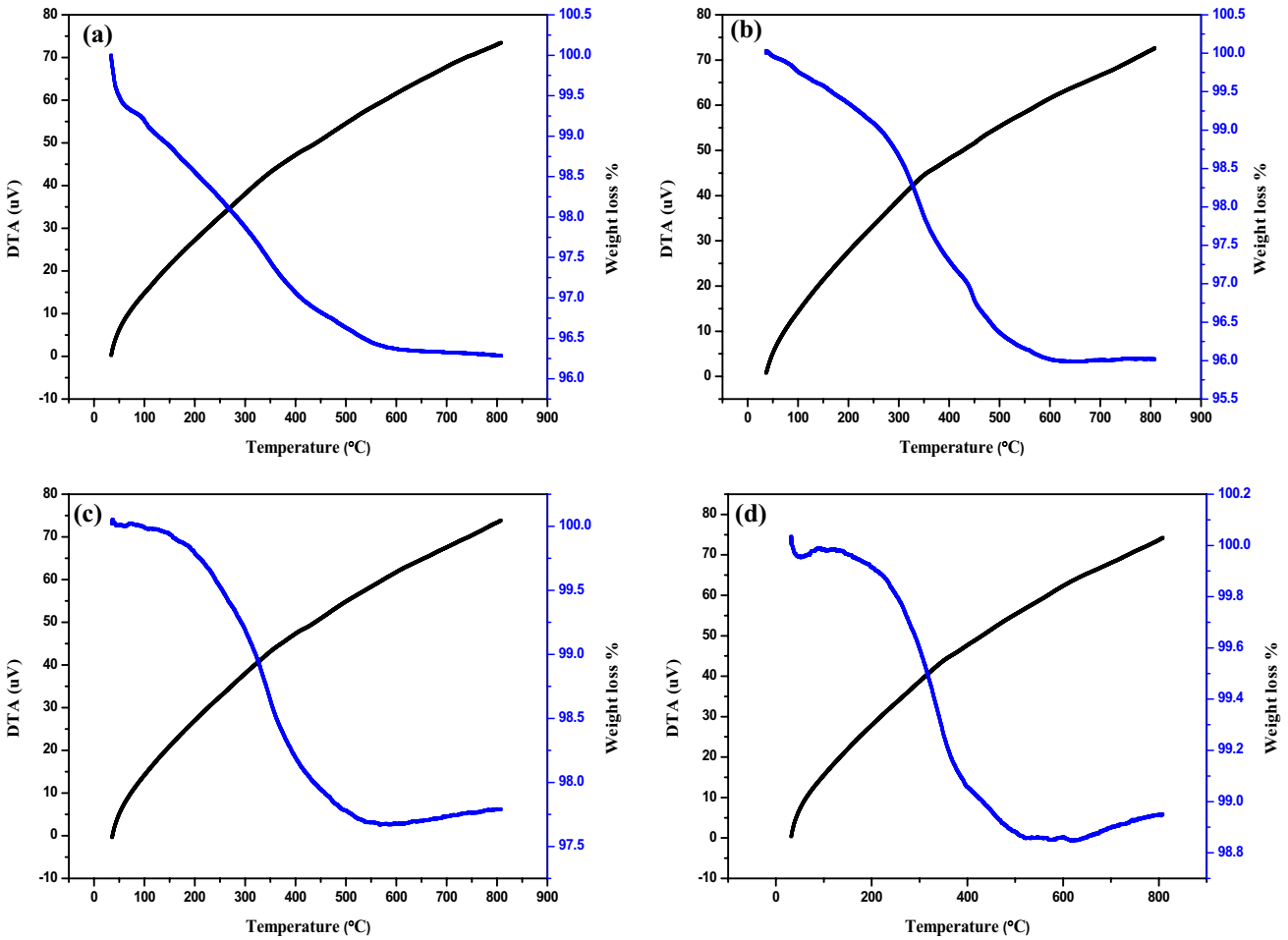

Fig. 4 TG curves of pure and In doped La_2CuO_4 nanoparticles

3.4 FTIR Studies

Figure 5 presents the infrared spectra of the LC samples, measured in the wavelength range of 4000–400 cm^{-1}. The FTIR spectrum investigations were conducted to examine the surface functional groups and the presence of perovskite structures. The water molecules that have been adsorbed exhibit a wide spectral band with a central peak at around 3420 cm^{-1}, which is linked to the stretching vibrations of the O-H bonds [20]. The O-O bonds exhibit lower intensity bands at 2923 and 2857 cm^{-1}, while the H-O-H bonds show bands at 1732 and 1648 cm^{-1}. The intense peak observed at 1526 and 1385 cm^{-1} in the residual nitrogen group can be attributed to the combustion route used for material synthesis [21, 22]. The presence of stretching modes is verified by the observed bands at 1188, 1113, 682, and 626 cm^{-1}, which can be attributed to the Cu-O bond. Moreover, the presence of two peaks at 523 and 438 cm^{-1}, linked to the La-O stretching modes, confirms the production of the perovskite phase in the orthorhombic La_2CuO_4, respectively [23].

3.5 Optical Properties

The LC system samples room-temperature UV-visible diffuse reflectance spectra were studied at the wavelength (λ) of 200–800 nm in order to explore the optical properties. The optical band gap energy was estimated using diffuse reflectance studies. By applying the modified Tauc relation Eq. (3), the optical band gap energy was determined.

$$F(R)h\nu = A(h\nu - Eg)^n \tag{3}$$

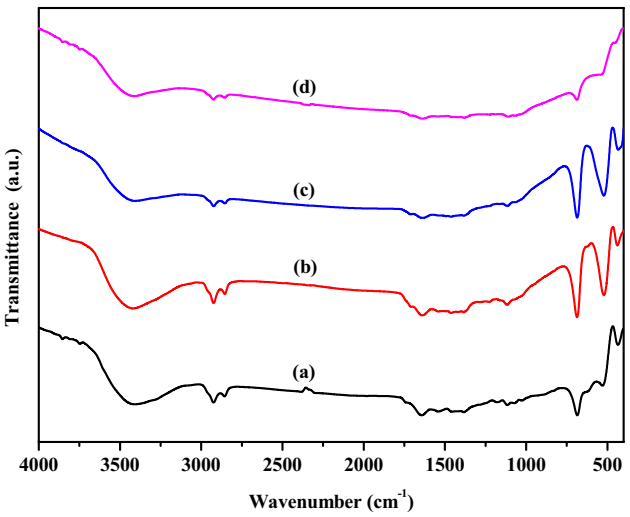

Fig. 5 The infrared spectra of the LC samples, measured in the wavelength range of 4000–400 cm^{-1}

where $n = 1/2$ and 2 represent direct and indirect transitions, thereby giving direct and indirect band gaps, respectively. The Kubelka–Munk function *[F(R)]* is generally applied to convert the diffuse reflectance into equivalent absorption coefficient (α) as given eqn. and mostly used for analyzing the powder samples.

$$\alpha = F(R) = \frac{(1-R)^2}{2R} \tag{4}$$

where *F(R)* is the Kubelka–Munk function; α is the photon absorption coefficient; *R* is the reflectance. A chart is plotted between $[F(R)h\nu]^2$ and hν. Figure 6 shows the direct band gap values which are given by the extrapolation of the linear region of the above plots to $[F(R)h\nu]^2 = 0$. The LSC nanosized samples estimated band gap energy values are 1.70, 1.71, 1.72, and 1.73 eV for $x = 0$, 0.05, 0.15, and 0.25, respectively. Because of the quantum confinement effect that takes place in the nano-regime, the pure LC sample gets a higher band gap value (1.88 eV) given in Table 1 than the reported value (1.30 eV) and (1.24 eV) [1, 24]. The doping of In^{3+} causes a decrease in the ratio of lanthanum compared to the indium host. This indicates that the LaO_2 layers will compress, leading to an increase in bond mismatch. Consequently, the LC crystallite samples exhibit an elevated band gap value.

3.6 Morphology Studies

Figure 7 shows lanthanum cuprate (LC) systems surface morphology. With the help of the combustion method, the doped and undoped LC nanoparticles were prepared, which involved an outbreak of H_2O molecule and easily vaporable gases like O_2, CO_2, and N_2, generating a simple structure in the LC systems with certain porosity. The samples reveal the development of nanoscaled crystalline grains with different shapes and pores. The undoped LC and In^{3+} doped La_2CuO_4 samples exhibit merged grains with distinct grain boundaries along the pore walls, whereas the pores consist of tiny, isolated grains. Figure 7 ($x = 0.05$ to 0.25) illustrates that the samples exhibit intragranular holes, with the particles being partially separate and merged with adjacent grains. Figure 8 displays the elemental composition for the LC sample system, which was estimated by using EDX (energy dispersive X-ray analysis). From the undoped La_2CuO_4 sample, the existence of oxygen (O), lanthanum (La), and copper (Cu) were confirmed using EDX analysis. Figure 8 ($x = 0.05$ to 0.25) depicts the peaks of La, In, Cu, and O elements present in the In^{3+} doped La_2CuO_4 substances.

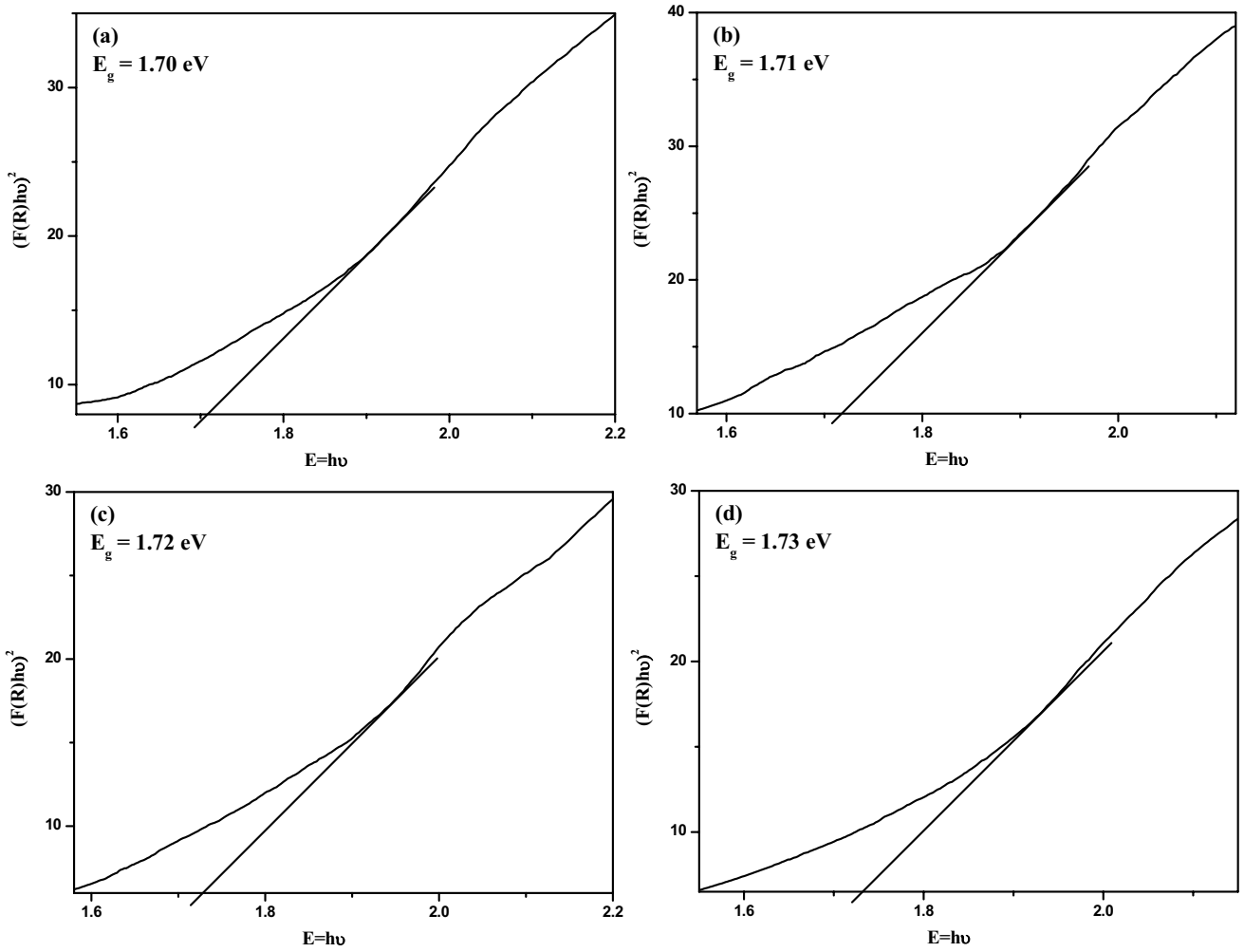

Fig. 6 The direct band gap values which are given by the extrapolation of the linear region

3.7 Magnetic Properties

The hysteresis curve for the magnetization-field (M-H) of the LC samples is depicted in Fig. 9. Under a 1.5 Tesla magnetic field at room temperature, the sample shows Ferro/para magnetic behavior (Table 2). Because the magnetization of the substance reaches saturation, it is predicted that the ferro/para magnetic characters will predominate as the perturbed magnetic field increases. The impact of In^{3+}, the saturation magnetization (M_s), changes drastically with indium content and reaches a maximum of 3.153–0.181 emu/g. The In^{3+} doping is responsible for the interchange of A and B sites in the LS host, which results in the fluctuation of magnetization. According to Upadhyay et al. [25], magnetization values exhibit rapid changes at a specific critical doping concentration. The transition from multi-domain to single-domain occurs at the critical size. Table 2 shows the correlation between coercivity (H_c) and remanence magnetization (M_r) with the crystallite size. H_c and M_r sharply decrease to minimum values among other doping levels (208.07–413.27 Oe and 0.415−0.022 emu/g), while starting to raise up again with a further decrease in crystallite size [26, 27].

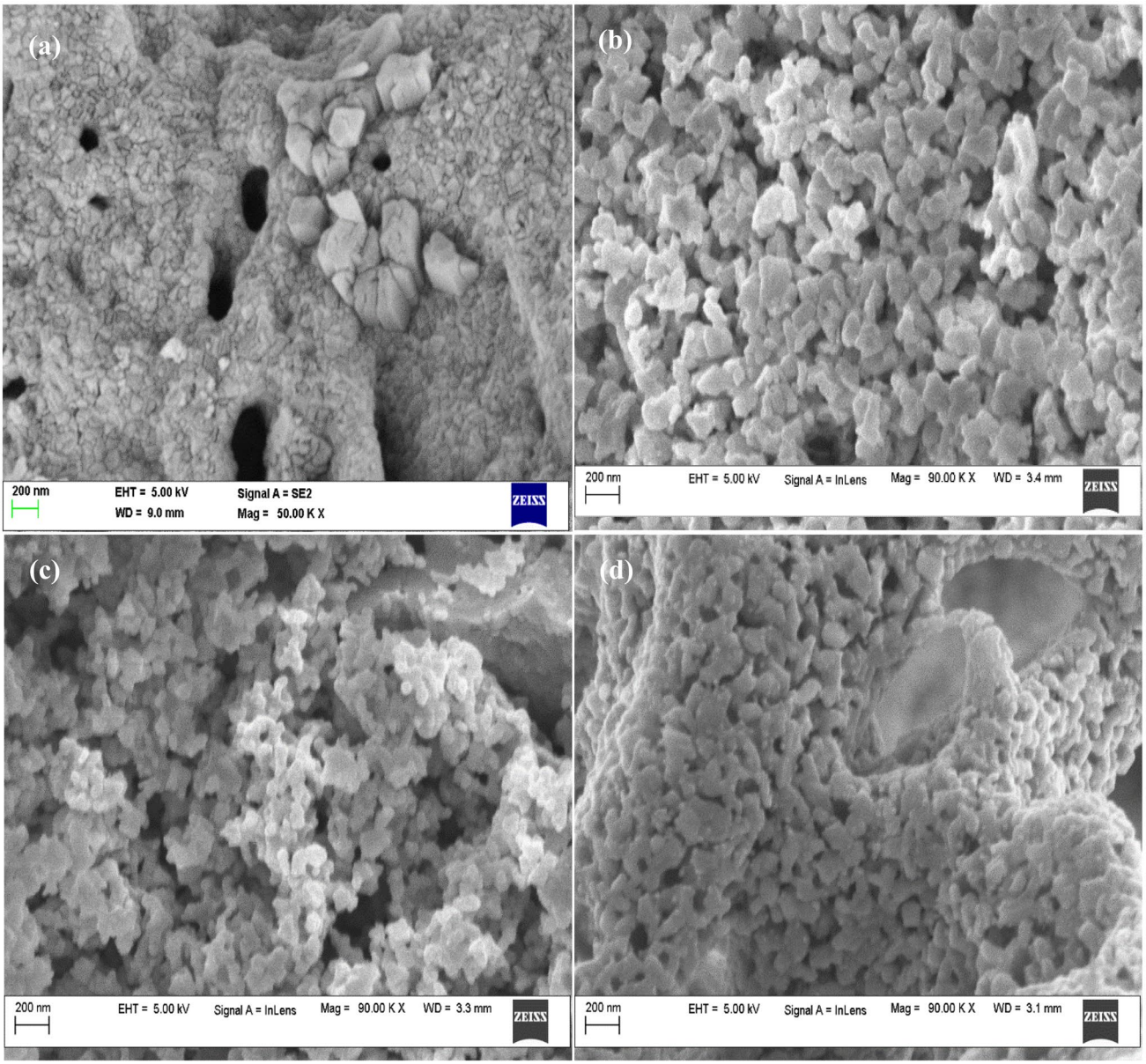

Fig. 7 The lanthanum cuprate (LC) systems surface morphology

The ionic radii for In^{3+} and La^{3+} are 0.81 and 1.06 Å which are in close proximity, so the replacement of lanthanum by indium will not bring about lattice deformation, which can produce some kind of point defects (voids). Meantime, indium has + 3 valance, while that of lanthanum has + 3 valance, which states that the exchange of La^{3+} by In^{3+} will bring about an uneven total charge of the substance (lack of positive charge) that generates certain voids (Oxygen) [28, 29]. The constitutional behavior described above can potentially have direct and indirect effects on

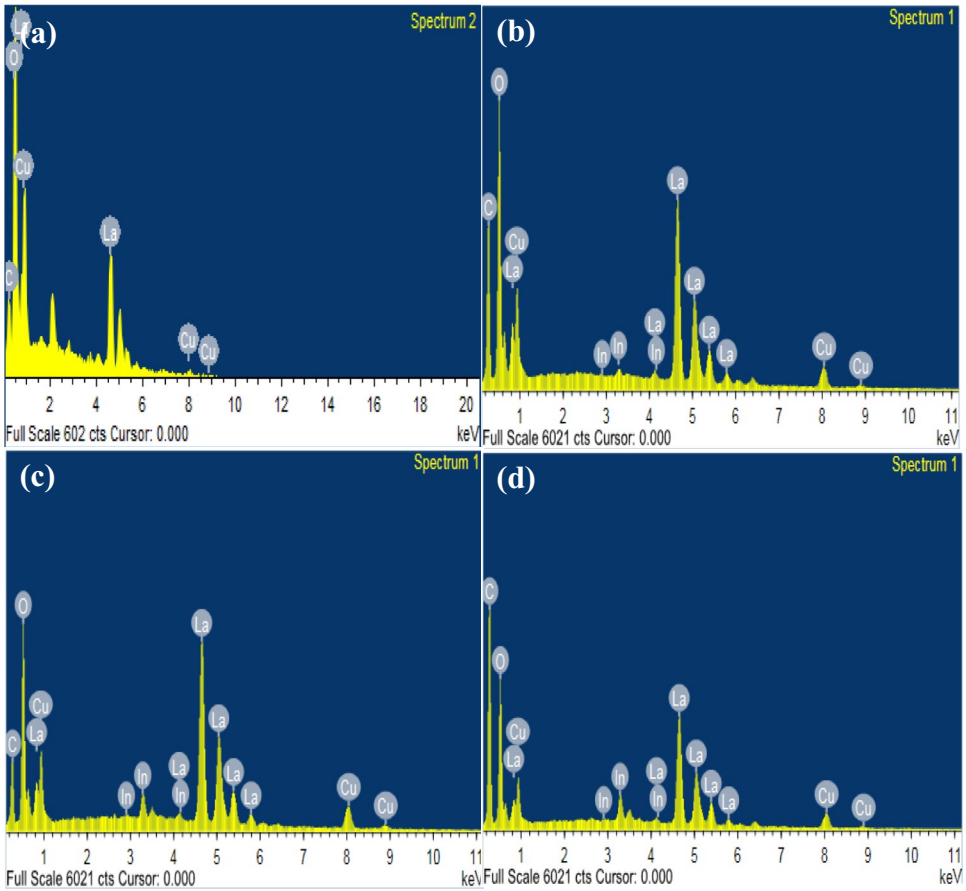

Fig. 8 The elemental composition for the LC sample system

the development of the properties and magnetic behavior of In^{3+} doped La_2CuO_4 grains. The effects discussed in this study are caused by the formation of vacancies (point defects) [30, 31], the substitution of La^{3+} with In^{3+} which displays paramagnetic properties, and the interactions between ions including O^{2-}, La^{3+}, In^{3+}, and Cu^{2+} at both long and short range.

Table 2 Coercivity (H_c), remanent magnetization (M_r), and saturation magnetization (M_s) values of $La_{2-x}In_xCuO_4$ ($x=0.0$, 0.05, 0.15, and 0.25) nanoparticles

Sample	Sample code	H_c (O_e)	M_r (emu/g)	M_s (emu/g)
La_2CuO_4	a	208.07	0.415	3.153
$La_{1.95}In_{0.05}CuO_4$	b	265.31	0.022	0.173
$La_{1.85}In_{0.15}CuO_4$	c	230.40	0.027	0.181
$La_{1.75}In_{0.25}CuO_4$	d	413.27	0.058	0.300

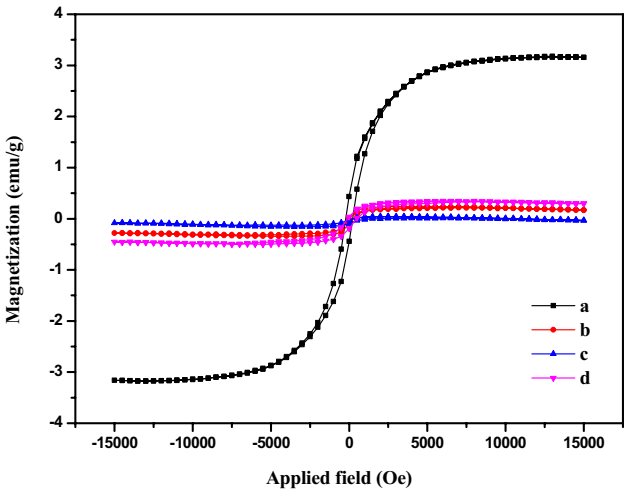

Fig. 9 The hysteresis curve for the magnetization-field (M-H) of the LC samples

4 Conclusion

$La_{2-x}In_xCuO_4$ nanoparticles were synthesized by the combustion method. With a rise in the doping of indium content from $x = 0.05$ to 0.25 and the phase orthorhombic studied using the Rietveld and XRD method. Rietveld refinement analyses are done by using the FULLPROF program. The refinement was carried out in the *Bmab* space group. As there is an increase in In^{3+} content porosity percentage also increases. The vibrational stretching frequencies of the La_2CuO_4 perovskite structure are confirmed by FTIR spectroscopy. The undoped and doped La_2CuO_4 energy band gap values 1.70–1.73 eV due to the quantum confinement. The SEM images revealed the existence of well-developed porosity and nanosized granules on the surfaces. RT magnetization tests demonstrated the presence of ferro/para magnetism phenomena.

Acknowledgements The authors extend their sincere appreciation to the Researchers Supporting Project number (RSP2024R370), King Saud University, Riyadh, Saudi Arabia for the support.

Author Contribution (1) Conceptualization: M. Sundararajan, Chandra Sekhar Dash; (2) methodology: S. Yuvaraj, P Aji Udhaya, R S Rimal Isaac; (3) formal analysis: Manish Gupta, Kirtanjot Kaur, Ala Manohar; (4) resources: Mohd Ubaidullah, S. Yuvaraj, Shoyebmohamad F. Shaikh; (5) writing—original draft: Chandra Sekhar Dash, M. Sundararajan; (6) writing—review and editing: Chandra Sekhar Dash, S. Yuvaraj; (7) visualization: P Aji Udhaya, M. Sundararajan, S Baskar.

Data Availability No datasets were generated or analysed during the current study.

Declarations

Competing Interests The authors declare no competing interests.

References

1. Li, Y., Huang, J., Cao, L., Wu, J., Fei, J.: Optical properties of La_2CuO_4 and $La_{2-x}Ca_xCuO_4$ crystallites in UV–vis–NIR region synthesized by sol–gel process. Mater. Charact. **64**, 36–42 (2012)
2. Velasquez, M., Santamaria, A., Batiot-Dupeyrat, C.: Selective conversion of glycerol to hydroxyacetone in gas phase over La2CuO4 catalyst. Appl. Catal. B Environ. **160–161**, 606–613 (2014)
3. Zhou, X., Cao, Q., Hu, Y., Gao, J., Xu, Y.: Sensing behavior and mechanism of La_2CuO_4- SnO_2 gas sensors. Sens. Actuators B Chem **77**, 443–446 (2001)
4. Tu, Q.Y., Chen, X.L., Ma, B.K., Zhao, Z.X., Li, J.Q., Liang, J.K.: Structural and superconducting properties of $La_2CuO_{4+\delta}$ chemically oxidized by NaClO. Phys. C Supercond. Its. Appl. **370**, 94–100 (2002)
5. Zhu, J., Zhao, Z., Xiao, D., Li, J., Yang, X., Wu, Y.: Characterization and catalytic activity in NO decomposition of $La_{2-x}Sr_xCuO_4$ ($0 \le x \le 1$) compounds with T* phase structure. Mater. Chem. Phys. **94**, 257–260 (2005)
6. Chen, X., Tang, K., Zeng, S., Hao, Q., Wang, D., Gao, Z., Wang, Y.: Fluorination of La_{2-x} Sr_xCuO_4 ($x = 0$, 0.15, 0.3) and study on the crystal structures, magnetic properties of their fluorinated products. J. Alloys Compd. **626**, 239–244 (2015)
7. Moodenbaugh, A.R., Wildgruber, U., Wang, Y.L., Xu, Y.: Hole doping in $La_{2-x}Ba_xCuO_{4-y}$ using oxygen stoichiometry. Phys. C Supercond. **245**(3–4), 347–354 (1995)
8. Zhao, Y., Gaulin, B.D., Castellan, J.P., Ruff, J.P.C., Dunsiger, S.R., Gu, G.D., Dabkowska, H.A.: High-resolution X-ray scattering studies of structural phase transitions in underdoped $La_{2-x}Ba_xCuO$. Phys. Rev. B **4**, 184121 (2007)
9. Crawford, M.K., Harlow, R.L., Deemyad, S., Tissen, V., Schilling, J.S., McCarron, E.M., Tozer, S.W., Cox, D.E., Ichikawa, N., Uchida, S., Huang, Q.: High-pressure study of structural phase transitions and superconductivity in $La_{1.48}Nd_{0.4}Sr_{0.12}CuO_4$. Phys. Rev. B **71**, 104513 (2005)
10. Tavana, A., Akhavan, M., Draxl, C.: First-principles study on lattice instabilities and structural phase transitions in Ba doped La_2CuO_4. Phys. C Supercond. Its. Appl. **517**, 20–25 (2015)
11. Kour, S., Jasrotia, R., Puri, P., Verma, A., Sharma, B., Singh, V.P., Kumar, R., Kalia, S.: Improving photocatalytic efficiency of $MnFe_2O_4$ ferrites via doping with Zn^{2+}/La^{3+} ions: photocatalytic dye degradation for water remediation. Environ. Sci. Pollut. Res. **30**, 71527–71542 (2023)
12. Gao, L., Wang, X., Tong Chua, H., Kawi, S.: Growth of La_2CuO_4 nanofibers under a mild condition by using single walled carbon nanotubes as templates. J. Solid State Chem. **179**, 2036–2040 (2006)
13. Sukumar, M., John Kennedy, L., Judith Vijaya, J., Al-Najar, B., Bououdina, M.: Facile synthesis of Fe^{3+} doped La_2CuO_4/$LaFeO_3$ perovskite nanocomposites: structural, optical, magnetic and catalytic properties. Mater. Sci. Semicon. Process. **100**, 225–235 (2019)
14. Sukumar, M., John Kennedy, L., Judith Vijaya, J., Al-Najar, B., Bououdina, M.: Structural, magnetic and catalytic properties of $La_{2-x}Ba_xCuO_4$ ($0 \le x \le 0.5$) perovskite nanoparticles. Ceram. Int. **44**, 18113–18122 (2018)
15. Huang, Z., Liu, J., Huang, L., Tian, L., Wang, S., Zhang, G., Li, J.: One-step synthesis of dandelion-like lanthanum titanate nanostructures for enhanced photocatalytic performance. NPG Asia Mater. **12**, 11 (2020)
16. Revathi, R., Ashok, A., Anitha, G., Kumar, A., Sukumar, M., Revathi, S., AlEnizi, A.M., Sundararajan, M., Pandit, B., Gupta, M., Dash, C.S., Yuvaraj, S., Ubaidullah, M.: Impact of In^{3+} doped $BiFeO_3$ nanoparticles prepared by direct combustion method: structurlemental, optical, vibrational, morphology and magnetic studies. J. Mater. Sci: Mater. Electron. (2024). https://doi.org/10.1007/s10854-023-11821-9
17. Rajadurai, L., Dash, C.S., Revathi, S., Tony Dhiwahar, A., Sundararajan, M., Ravisankar, P., Alagarasan, J.K., Mohandoss, S., Sambasivam, R.: Photocatalytic degradation of tetracycline hydrochloride using pure and copper-doped magnesium ferrite nanoparticles: efficiency, kinetics and mechanism. Inorgan Chem. Commun. **162**, 112197 (2024)
18. Narsimulu, D., Nageswara Rao, B., Venkateswarlu, M., Srinadhu, E.S., Satyanarayana, N.: Electrical and electrochemical studies of nanocrys-talline mesoporous $MgFe_2O_4$ as anode material for lithium battery applications. Ceram. Inter. **42**(15), 16789–16797 (2016)
19. Baskar, S., Yuvaraj, S., Sundararajan, M., Dash, C.S.: Influence of Ca^{2+} ion substitution on structural, morphological, optical, thermal and magnetic behaviour of $Mg_{1-x}Ca_xFe_2O_4$ ($0 \le x \le 0.5$) Spinel. J. Supercond. Novel Magnetism. (2020). https://doi.org/10.1007/s10948-020-05665-1
20. Sundararajan, M., Kennedy, L.J., Aruldoss, U., Pasha, S.K., Vijaya, J.J., Dunn, S.: Microwave combustion synthesis of zinc substituted nanocrystalline spinel cobalt ferrite: structural and magnetic studies. Mater. Sci. Semicond. Process. **40**, 1–10 (2015)

21. Yuvaraj, S., Roniboss, A., Kumar, A.: Microwave combustion synthesis of $La_{1-x}Gd_xFeO_3$ ($x = 0$ *to* 0.25) nanoparticles: structural, magnetic, vibrational, morphology and optical behavior. J. Inorg. Organomet. Polym. (2024). https://doi.org/10.1007/s10904-023-02840-4
22. Dharmadhikari, D.V., Nikam, S.K., Athawale, A.A.: Template free hydrothermal synthesis and gas sensing application of lanthanum cuprate (La_2CuO_4): Effect of precursors on phase formation and morphology. J. Alloy Compd. **590**, 486–493 (2014)
23. Sukumar, M., Kennedy, L.J.: Catalytic conversion of methanol to formaldehyde over La_2CuO_4 nanoparticles. J. Nanosci. Nanotechnol. **19**, 826–832 (2019)
24. Enhessari, M., Shaterian, M., Esfahani, M.J., Motaharian, M.N.: Synthesis, characterization and optical band gap of La_2CuO_4 nanoparticles. Mater. Sci. Semicond. Process **16**, 1517–1520 (2013)
25. Upadhyay, K.: Parekh: Influence of crystallite size on the magnetic properties of Fe3O4 nanoparticles. J. Alloy Comp. **678**, 478–485 (2016)
26. Kaur, S., Chalotra, V.K., Jasrotia, R., Bhasin, V., Suman, S., Kumari, S., Thakur, J., Ahmed, A., Mehtab, T., Ahmad, R., Singh, S.K.: Godara: Spinel nanoferrite (CoFe2O4): The impact of Cr doping on its structural, surface morphology, magnetic, and antibacterial activity traits. Opt. Mater. **133**, 113026 (2022)
27. Sharma, H.R., Batoo, K.M., Sharma, P., Bhardwaj, S., Kuchhal, P., Jasrotia, R., Sharma, I., Kumar, G.: Structural, electrical, and magnetic studies of Cu^{2+} substituted $MnFe_2O_4$ nanoferrites synthesized via solution combustion technique. J. Mater. Scien Mater. Electron. **33**, 7528–7542 (2022)
28. Jasrotia, R., Singh, V.P., Sharma, R.K., Kumar, P., Singh, M.: Analysis of effect of Ag+ ion on microstructure and elemental distribution of strontium W-type hexaferrites. AIP Conf. Proc. **2142**, 140004 (2019)
29. Jasrotia, R., Kumari, N., Verma, R., Godara, S.K., Ahmed, J., Alshehri, S.M., Pandit, B., Kumar, S., Sharma, S., Maji, P.K.: Effect of rare earth (Nd3+) metal doping on structural, morphological, optical and magnetic traits of Zn–Mg nano-ferrites. J. Rare Earths. **41**, 1763–1770 (2023)
30. Sukumar, M., Agila, M., Sutha, A., Ravi, V., Al-Enizi, A.M., Ubaidullah, M., Samdani, M.S., Sundararajan, M., Pandit, B.: Temperature-dependent phase transition: Structural, optical, magnetic and dielectric properties La_2CuO_4 perovskite nanoparticles. J. Mater. Scien Mater. Electron. **33**, 26144–26156 (2022)
31. Sundararajan, M., Bonisha, B., Ubaidullah, M., Shaikh, S.M.F., Revathi, S., Thiripurasundari, D., Dhiwahar, A.T., Pandit, B., Dash, C.S., Shahazad, M.: Enhanced visible light photocatalytic degradation of rhodamine B using $Ni_{1-x}Ca_xFe_2O_4$ ($0 \le x \le 0.5$) nanoparticles: Performance, kinetics and mechanism. Mater. Res. Bull. **154**, 111911 (2022)